Paper 75-4 has been designated as a Distinguished Student Paper at Display Week 2025. The full-length version of this paper appears in a Special Section of the *Journal of the Society for Information Display (JSID)* devoted to Display Week 2025 Distinguished Papers. This Special Section will be freely accessible until December 31, 2025 via:

https://sid.onlinelibrary.wiley.com/doi/full/10.1002/jsid.2061

Authors that wish to refer to this work are advised to cite the full-length version by referring to its DOI:

https://doi.org/10.1002/jsid.2061

Fast-Switchable Polarization-Dependent Bifocal Lenses for AR Displays

Ming Cheng[1,2], Vigneshwaran Swaminathan[1], Yuxiao Zhang[2], Chris Mathew[1], Valerii Vashchenko[1], Yan Jun Liu[2,] and Abhishek K. Srivastava[1,*]*

[1] State Key Laboratory of Advanced Displays and Optoelectronics Technologies, Center for Display Research, and IAS Center for Quantum Technologies, Department of Electronic and Computer Engineering, Hong Kong University of Science and Technology, Hong Kong 999077, China

[2] Department of Electronic and Electrical Engineering, Southern University of Science and Technology, Shenzhen 518055, China

Abstract

Polarization-dependent bifocal Pancharatnam-Berry phase lenses are proposed to integrate bifocal functions into a single device. These lenses, fabricated using photoalignment techniques, are designed in both longitudinal and transverse configurations to address key challenges in AR displays. The longitudinal configuration resolves the vergence-accommodation conflict through multi-plane displays, while the transverse configuration enlarges the field-of-view (FOV) by enabling dual horizontal FOVs. The system also incorporates an electrically suppressed helix ferroelectric liquid crystal polarization rotator, enabling fast switching between dual depths or FOVs. This compact, efficient solution addresses key challenges in AR displays, allowing true 3D multi-plane displays and extending the FOV for next-generation AR systems.

1. Introduction

Augmented reality (AR) displays enable the interaction of virtual images with the real world, providing enhanced visual information and experiences across various fields, such as healthcare, education, entertainment, and the military. As AR technology continues to advance, optimizing key performance factors, including the vergence-accommodation (VA) conflict, field of view (FOV), eye box size, and image brightness, remains a significant focus.

A critical challenge in AR systems is the VA conflict, which arises from the fixed focal distance in most existing devices. The conflict occurs due to the binocular stereoscopic technique for 3D displays, which mismatches the vergence distance with the accommodation distance, leading to discomfort and visual strain. Multi-plane display techniques have emerged as a promising solution to generate 3D images by establishing multiple 2D image slices at different depths to address this issue. Recent advancements include distance-based [1-3] and power-based methods [4,5], which utilize optical path differences and tunable optical power, respectively. For instance, Chen et al. proposed a multi-plane AR display using two cholesteric liquid crystal reflective films positioned at different depths [3]. In contrast, power-based systems tend to be simpler and more compact. Li et al. developed a dual-depth AR system employing polarization-dependent reflective off-axis Pancharatnam-Berry (PB) phase lenses [5]. Another key factor in AR systems is the FOV. To increase the FOV and reduce the aberration caused by the low f-number of the combiner lens, Yin et al. propose a polarization-dependent method to double the FOV using two reflective off-axis PB lenses [6].

It's worth noting that the PB phase lenses mentioned above have emerged as potential candidates for next-generation flat optical components due to their flat properties, polarization-dependent response, and high efficiency. However, existing setups based on polarization-dependent effects typically involve two effective optical components that respond to different polarization states [3,5,6]. Integrating these functions into a single device would be highly advantageous for a compact system. Additionally, response time is a critical factor; in multi-plane displays, the various planes must switch fast enough to avoid detection by human eyes to achieve a convincing 3D display. When switching is used to adjust the horizontal FOV, the speed must be fast enough to make the FOV appear simultaneously, thereby achieving the function of extending the FOV. Achieving rapid switching, especially for multiple depths and larger FOVs, places high demands on new materials and strategies.

Here, we propose polarization-dependent bifocal lenses that integrate bifocal functions into a single device. These devices are based on a specialized phase design and are fabricated using photoalignment techniques that assist with spatially patterned polarized light fields generated by a spatial light modulator (SLM). Both longitudinal and transverse configurations are designed to address distinct challenges in AR systems, as illustrated in Figure 1. The longitudinal one provides dual-depth capabilities for 3D displays, resolving the VA conflict, while the transverse one enables left and right FOVs, effectively enlarging the overall FOVs. Furthermore, both configurations are combined with an electrically suppressed helix ferroelectric liquid crystal (ESHFLC) polarization rotator, allowing fast switching between two depths or views. This rapid switching enhances the effectiveness of true 3D multi-plane displays and expands the FOV of the entire system. Our proposed strategy significantly compacts the system while achieving fast response, offering a promising solution to existing challenges in AR systems.

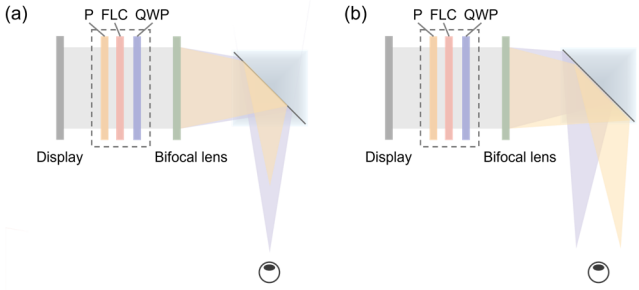

Figure 1. Schematic illustration of AR system utilizing designed (a) longitudinal bifocal lens and (b) transverse bifocal lens.

2. Design strategy

The bifocal lens is designed following the holographic principle and geometric phase [7]. The interference between left circularly polarized (LCP) light and right circularly polarized (RCP) light, each carrying its respective focusing information in the phase, can be recorded and subsequently reconstructed. These two light fields can be expressed as

$$E_{LCP} = A_1 e^{-i\frac{2\pi}{\lambda}\left(\sqrt{(x-x_1)^2+(y-y_1)^2}-f_1\right)},$$
$$E_{RCP} = A_2 e^{i\frac{2\pi}{\lambda}\left(\sqrt{(x-x_2)^2+(y-y_2)^2}-f_2\right)},$$

ISSN 0097-996X/25/5602-1024-$1.00 © 2025

where λ is the wavelength, A_1 and A_2 are the respective amplitude, (x_1, y_1) and (x_2, y_2) are the positions of the respective focal points, f_1 and f_2 are the focal lengths of the two light fields. By superimposing these two light fields, the designed phase can be extracted. In our case, $A_1 = A_2 = 1$. The two focal lengths for the longitudinal bifocal lens are set at 150 mm and 300 mm, respectively. For the transverse bifocal lens, the focal length is fixed at 500 mm, with the focal points separated by 3 mm.

The geometric phase (φ) required for this lens design can be achieved using birefringent LC molecules, whose orientation angle (θ) is related to the phase following $\varphi = 2\theta$ when the half-wave condition is satisfied. Consequently, the molecular alignment can be patterned to match the phase distribution, allowing for the desired light field modulation. The photoalignment technique is employed to pattern the LC molecules, utilizing an SLM-based system, as shown in Figure 2(a). This system consists of a polarizer, a SLM with tunable phase retardation, rotated 45° with respect to the polarizer, and a quarter-wave plate (QWP) aligned with the polarizer. The output light passing through the system can be expressed using the Jones Matrix [8]:

$$E_{out} = M_{QWP} M_{SLM}\, M_{polarizer} E_{in}$$

$$= \begin{bmatrix} e^{-i\frac{\pi}{4}} & 0 \\ 0 & e^{i\frac{\pi}{4}} \end{bmatrix} \begin{bmatrix} cos45° & sin45° \\ -sin45° & cos45° \end{bmatrix} \begin{bmatrix} e^{-i\frac{\delta}{2}} & 0 \\ 0 & e^{i\frac{\delta}{2}} \end{bmatrix}$$

$$\begin{bmatrix} cos45° & -sin45° \\ sin45° & cos45° \end{bmatrix} \begin{bmatrix} 0 & 0 \\ 0 & 1 \end{bmatrix} \begin{bmatrix} E_x \\ E_y \end{bmatrix} = e^{i\frac{\pi}{4}} E_y \begin{bmatrix} sin\dfrac{\delta}{2} \\ cos\dfrac{\delta}{2} \end{bmatrix}$$

where δ is the phase retardation generated by the SLM. By tuing the electric field, which is quantized to the gray levels, the phase retardation can be adjusted to generate different polarization angles. The relationship between the gray level and polarization angle is measured and shown in Figure 2(b). Following the holographic phase design principles, the gray levels for the designed longitudinal and transverse bifocal lenses are presented in Figure 2(c) and 2(d), respectively.

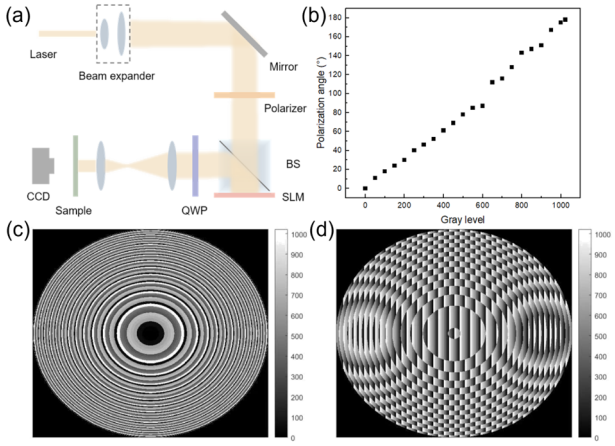

Figure 2. SLM-based photoalignment system. (a) Schematic illustration of the system's optical path. (b) Relationship between the output polarization angle and the SLM gray level. Designed gray level distributions for (c) the longitudinal bifocal lens and (d) the transverse bifocal lens.

The ESHFLC polarization rotator's operation can be simplified to a half-wave plate with an effective optical axis that rotates in the plane driven by the applied electric field. When incident light passes through a polarizer, the EHSFLC cell, and a 45° rotated QWP, as shown in Figure 3(a), the modulated light can be represented by the following Jones matrix:

$$E_{out} = M_{QWP} M_{FLC}\, M_{polarizer} E_{in}$$

$$= \begin{bmatrix} cos45° & sin45° \\ -sin45° & cos45° \end{bmatrix} \begin{bmatrix} e^{-i\frac{\pi}{4}} & 0 \\ 0 & e^{i\frac{\pi}{4}} \end{bmatrix} \begin{bmatrix} cos45° & -sin45° \\ sin45° & cos45° \end{bmatrix}$$

$$\begin{bmatrix} cos\alpha & sin\alpha \\ -sin\alpha & cos\alpha \end{bmatrix} \begin{bmatrix} e^{-i\frac{\delta}{2}} & 0 \\ 0 & e^{i\frac{\delta}{2}} \end{bmatrix} \begin{bmatrix} cos\alpha & -sin\alpha \\ sin\alpha & cos\alpha \end{bmatrix} \begin{bmatrix} 0 & 0 \\ 0 & 1 \end{bmatrix} \begin{bmatrix} E_x \\ E_y \end{bmatrix}$$

where $\alpha = \beta + \Delta\theta$ is the axis angle of ESHFLC with respect to the polarizer, β corresponds to the initial alignment, $\Delta\theta$ is the induced tilt angle due to the applied electric field relative to the initial alignment, and δ is the phase retardation. If δ is designed to satisfy half-wave condition and is assumed to be approximately constant when different voltage is applied, which means $\delta = \pi$, the output light can be calculated as

$$E_{out} = e^{-i\frac{\pi}{4}} E_y \begin{bmatrix} sin2(\beta + \Delta\theta) + icos2(\beta + \Delta\theta) \\ isin2(\beta + \Delta\theta) + cos2(\beta + \Delta\theta) \end{bmatrix}$$

Since ESHFLCs exhibit binary behavior when the voltage is applied, the director can be reoriented in opposite directions depending on whether a positive or negative voltage is used due to their polar nature. If the initial alignment angle β is set to be 22.5° and the tilt angle $\Delta\theta$ is also designed to be 22.5°, then under a positive voltage, $\beta + \theta_{ind}$=22.5°+22.5°=45°, illustrated in Figure 3(b). In this case, the output light is represented by

$$E_{out} = \frac{1}{2} e^{-i\frac{\pi}{4}} E_y (i+1) \begin{bmatrix} 1 \\ i \end{bmatrix}$$

which corresponds to LCP. For the other state, under a negative voltage, $\beta + \theta_{ind}$=22.5°-22.5°=0°, illustrated in Figure 3(b), and the output light is given by

$$E_{out} = \frac{1}{2} e^{-i\frac{\pi}{4}} E_y (i+1) \begin{bmatrix} i \\ 1 \end{bmatrix} = \frac{1}{2} e^{-i\frac{\pi}{4}} E_y (i-1) \begin{bmatrix} 1 \\ -i \end{bmatrix}$$

which corresponds to RCP. Thus, by designing the driving signal to alternate between positive and negative voltages, polarization rotation between LCP and RCP can be achieved. A homemade material, FLC-11-044, is designed to exhibit exactly a 22.5° tilt angle at room temperature, and the cell gap is carefully controlled to achieve half-wave condition, meeting the requirements for polarization switching. A 90 Hz frequency driving signal is applied, as shown in Figure 3(c), with the corresponding response fast enough that the human eye cannot distinguish between the two states, perceiving them as occurring simultaneously. The response time relative to the applied voltage is shown in Figure 3(d). For the 5V driving, the response time is measured at 35 μs.

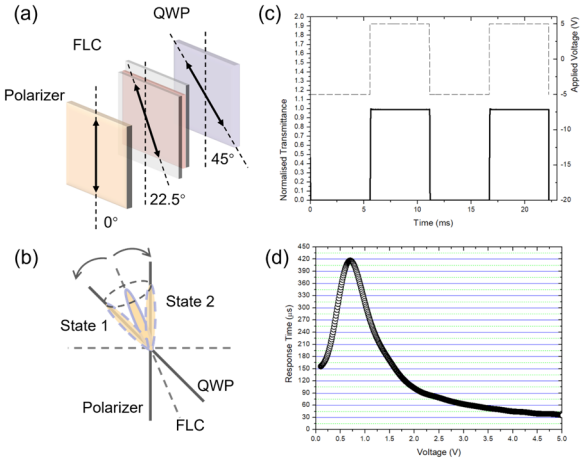

Figure 3. ESHFLC polarization rotator. (a) Schematic illustration of the optical components comprising the system and (b) their relationship. (c) Driving signal with a 90 Hz frequency and the corresponding response of the ESHFLC under cross polarizers. (d) Response time of ESHFLC relative to the applied voltage.

3. Results

The designed longitudinal and transverse bifocal lenses are fabricated using a multi-step process that includes photoalignment layer exposure, liquid crystal polymer (LCP) coating, and subsequent polymerization. To optimize focusing efficiency, the thickness of the LCP layer is carefully controlled by adjusting the concentration of the LCP solution and the spin-coating speed, ensuring it meets the half-wave condition. The alignment of LC molecules within the lenses is characterized using polarized optical microscopy (POM), as shown in Figure 4. Under crossed polarizers, the resulting grayscale clearly reflects the alignment directions of LC molecules. The observed alignment patterns are consistent with the design, confirming the effectiveness of the SLM-based photoalignment fabrication process.

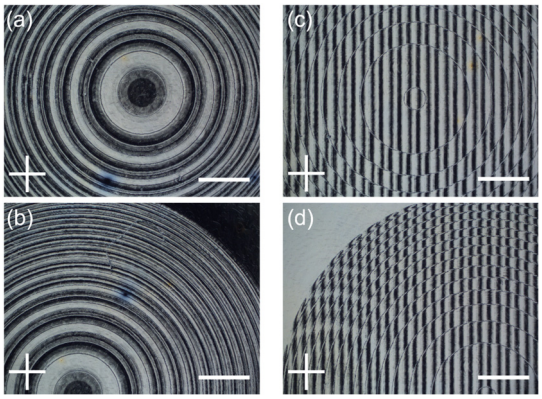

Figure 4. POM images of the fabricated (a) and (b) longitudinal bifocal lens, and (c) and (d) transverse bifocal lens. Scale bar: 500 μm.

The focusing effect is characterized using the setup shown in Figure 5(a). An expanded and collimated laser beam with a wavelength of 532 nm is directed onto the sample after passing through a polarizer and a QWP for circularly polarized light generation. The beam is adjusted using a tunable aperture to match the lens size (~4 mm). Switching between LCP and RCP is controlled by rotating the QWP. For the longitudinal bifocal lens, incident LCP and RCP light results in focal points at 300 mm and 150 mm, respectively, which is in agreement with the design. For the transverse bifocal lens, the collimated incident light is focused at two points on the plane at z=500 mm. Their respective light field distributions at the focal planes, shown in Figures 5(b) and 5(c), demonstrate a well-defined focusing effect, confirming the lens's performance. However, some efficiency loss is observed as a weaker focal point at the other focal plane, which could be further optimized.

Finally, the AR application is demonstrated for both dual-plane and dual-viewpoint displays. A display panel showing the letter "A" passes through a polarization rotation system consisting of a polarizer and a QWP, then through the designed bifocal lens, and enters the human eye via a beam splitter combiner. For the longitudinal bifocal lens, adjusting the polarization state of the incident light allows for two distinct focal planes, as shown in Figure 6(a). The images are captured by a camera with manual focus adjustment. For an LCP incident light, the "A" appears clearly on the plane corresponding to an object, which is a spaceman making a V-sign. For the RCP light, the "A" appears clearly on the plane, corresponding to a spaceman making a hi-sign. The two spacemen are positioned at different depths, with the V-sign spaceman located farther than the hi-sign spaceman. These results demonstrate the capability of the longitudinal bifocal lens for dual-plane display in AR. Furthermore, an ESHFLC polarization rotator is added between the polarizer and the QWP to enable electrically controlled dynamic polarization rotation. The driving signal is set to 500 Hz, and the display is captured by the camera at a 1/60 s shutter speed, mimicking the human eye's response, as shown in Figure 6(b). It's evident that the "A" remains clearly visible at both depths, demonstrating the fast switching between two planes and validating the potential for true 3D display in AR.

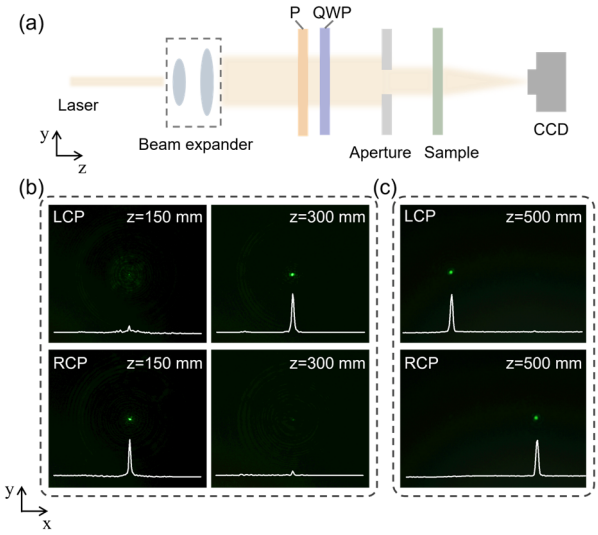

Figure 5. Focusing effect of the fabricated bifocal lens. (a) Schematic illustration of the characterization optical setup. The captured light field intensity distributions at the focal plane for (b) the longitudinal bifocal lens and (c) the transverse bifocal lens.

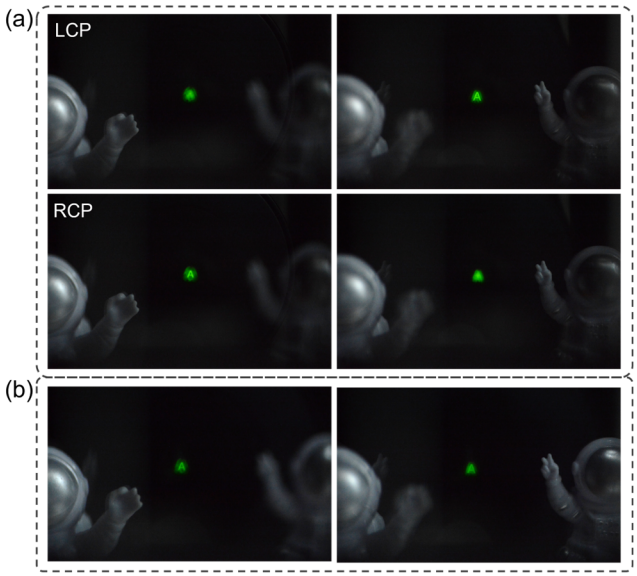

Figure 6. Dual-plane AR display using the longitudinal bifocal lens. (a) Images captured with a 1/60 s shutter speed camera through our AR display system, without the FLC polarization rotator, for LCP and RCP incident light. (b) Images captured through our AR system with the FLC polarization rotator for fast switching between LCP and RCP light.

The transverse bifocal lens is used to generate left and right FOVs, effectively enlarging the overall FOV. Without the FLC, polarization switching results in left and right two images shown on the same plane, but only one image is visible at a time, corresponding to one polarization, as shown in Figure 7(a). When the FLC is added to the system, its fast switching capability allows

the two images to switch rapidly enough to be recognized by a camera with a 1/60 s shutter speed, making both images appear simultaneously, as shown in Figure 7(b). This strategy fully utilizes polarization multiplexing and time multiplexing, with the FLC enabling fast switching to achieve an extended FOV.

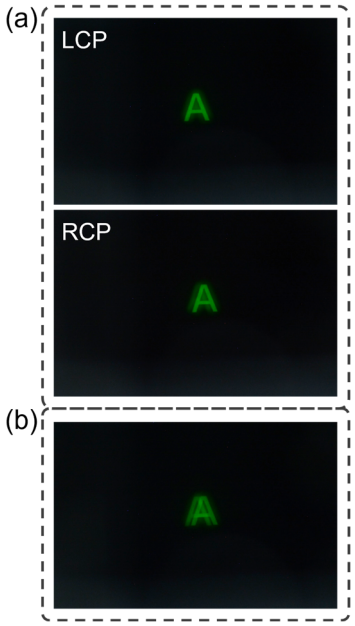

Figure 7. Dual-FOV AR display using the transverse bifocal lens. (a) Images captured with a 1/60 s shutter speed camera through our AR display system, without the FLC polarization rotator, for LCP and RCP incident light. (b) Images captured through our AR system with the FLC polarization rotator for fast switching between LCP and RCP light.

4. Discussion

By patterning the LC orientation using the photoalignment technique and SLM systems, the phase distribution can be designed to achieve arbitrary light field modulation in theory. Compared to interference-based methods [5,6], this approach offers greater design flexibility and requires less stringent exposure setup and environmental conditions. Using this technique, bifocal lenses are fabricated to enable dual-depths and dual-FOV AR display. However, due to the pixel size and diffraction limits, the resolution of SLM or digital micromirror device (DMD)-based photoalignment is constrained to around 1 μm, with a millimeter-scale fabrication area when focusing the beam through an objective lens [9]. As a result, the numerical aperture of the fabricated lenses is restricted, which is reflected in the limited FOV in the AR displays shown in Figures 6 and 7. Multi-step exposure and special fabrication techniques can be employed to optimize the device size and resolution [10]. Additionally, with advancements in nanofabrication techniques, metasurfaces are emerging as promising candidates for light field modulation based on phase design, targeting large-area and high-NA metalens.

Our proposed strategy, which incorporates polarization-dependent bifocal lenses and a fast FLC polarization rotator, offers an innovative solution to key challenges in AR systems and provides a proof-of-concept for further research. Notably, this strategy is also applicable to Maxwillian displays, where it can effectively expand the eyebox by establishing two viewpoints using the transverse bifocal lens. The system demonstrates a potential pathway toward achieving a more compact design compared to previous approaches [10-14], while enabling fast pupil steering to further simplify the system architecture.

5. Conclusion

In conclusion, the proposed polarization-dependent bifocal lenses, integrated with a fast FLC polarization rotator, offer an effective solution to key challenges in AR displays, including the VA conflict and limited FOV. By enabling dual depths and dual FOVs, the system provides a compact and efficient approach to achieving true 3D multi-plane displays and enhancing FOV while paving the way for the further application of fast viewpoint switching in Maxwellian displays.

6. Acknowledgments

We acknowledge the support of The Government of the Hong Kong Special Administrative Region, the Research Grants Council (RGC) for grant 16205623, and the Innovation and Technology Fund (ITF-ITS/059/22MX). We also acknowledge the support of The State Key Laboratory of Advanced Displays and Optoelectronics.

References

[1] Lee H, Peng F, Wu ST. Fast-response switchable lens for 3D and wearable displays. Optics Express. 2016;24(2):1668–1675.

[2] Liu S, Li Y, Zhou P, Chen Q, Su Y. Reverse-mode PSLC multi-plane optical see-through display for AR applications. Optics Express. 2018;26(3): 3394–3403.

[3] Chen Q, Peng Z, Li Y, Liu S, Zhou P, et al. Multi-plane augmented reality display based on cholesteric liquid crystal reflective films. Optics Express. 2019;27(9):12039-12047.

[4] Kumar MB, Kang D, Jung J, Park H, Hahn J, et al. Compact vari-focal augmented reality display based on ultrathin, polarization-insensitive, and adaptive liquid crystal lens. Optics and Lasers in Engineering.2020;128:106006.

[5] Li Y, Yang Q, Xiong J, Li K, Wu ST. Dual-depth augmented reality display with reflective polarization-dependent lenses. Optics Express.2021;29(20):31478-31487.

[6] Yin K, He Z, Li K, Wu ST. Doubling the FOV of AR displays with a liquid crystal polarization-dependent combiner. Optics Express. 2021;29(8):11512-11519.

[7] Zhou Y, Yuan Y, Zeng T, Wang X, Tang D, et al. Liquid crystal bifocal lens with adjustable intensities through polarization controls. Optics Letters. 2020;45(20):5716-5719.

[8] Li Y, Liu Y, Li S, Zhou P, Zhan T, et al. Single-exposure fabrication of tunable Pancharatnam-Berry devices using a dye-doped liquid crystal. Optics Express. 2019;27(6):9054-9060.

[9] Wei B, Hu W, Ming Y, Xu F, Rubin S, Wang J, Chigrinov V, Lu Y. Generating switchable and reconfigurable optical vortices via photopatterning of liquid crystals. Advanced Materials.2014;26(10):1590-1595.

[10] Guo Y, Jiang M, Peng C, Sun K, Yaroshchuk O, Lavrentovich O, Wei Q. High-resolution and high-throughput plasmonic photopatterning of complex molecular orientations in liquid crystals. Advanced Materials. 2016;28(12):2353-2358.

[11] Xiong J, Li Y, Li K, Wu ST. Aberration-free pupil steerable Maxwellian display for augmented reality with cholesteric liquid crystal holographic lenses. Optics Letters. 2021;46(7):1760-1763.

[12] Zou J, Li L, Wu ST. Gaze-matched pupil steering Maxwellian-view augmented reality display with large angle diffractive liquid crystal lenses. Advanced Photonics Research. 2022;3(5):2100362.

[13] Kim SB, Park JH. Optical see-through Maxwellian near-to-eye display with an enlarged eyebox. Optics Letters. 2018;43(4):767-770.

[14] Lin T, Zhan T, Zou J, Fan F, Wu ST. Maxwellian near-eye display with an expanded eyebox. Optics Express. 2020;28(26):38616-38625.